

# Dynamical instabilities of Bose-Einstein condensates at the band-edge in one-dimensional optical lattices

Andrew J. Ferris and Matthew J. Davis

*ARC Centre of Excellence for Quantum-Atom Optics, School of Physical Sciences,  
University of Queensland, Brisbane QLD 4072, Australia.*

Reece W. Geursen, P. Blair Blakie, and Andrew C. Wilson

*Jack Dodd Centre for Photonics and Ultra-Cold Atoms, Department of Physics,  
University of Otago, P.O. Box 56, Dunedin, New Zealand.*

(Dated: April 18, 2021)

We report on experiments that demonstrate dynamical instability in a Bose-Einstein condensate at the band-edge of a one-dimensional optical lattice. The instability manifests as rapid depletion of the condensate and conversion to a thermal cloud. We consider the collisional processes that can occur in such a system, and perform numerical modeling of the experiments using both a mean-field and beyond mean-field approach. We compare our numerical results to the experimental data, and find that the Gross-Pitaevskii equation is not able to describe this experiment. Our beyond mean-field approach, known as the truncated Wigner method, allows us to make quantitative predictions for the processes of parametric growth and thermalization that are observed in the laboratory, and we find good agreement with the experimental results.

PACS numbers: 03.75.Kk, 03.75.Lm, 05.10.Gg

## I. INTRODUCTION

Since the realization of dilute-gas Bose-Einstein condensates (BECs) [1, 2, 3] there have been many experiments on BECs in one-dimensional (1D) optical lattices [4, 5, 6, 7, 8, 9, 10, 11, 12, 13, 14, 15, 16, 17, 18, 19, 20]. Neutral atoms in periodic potentials demonstrate a wide range of phenomena that are familiar from other physical systems. Dilute gas BECs are attractive systems in which to study these effects due to the flexibility and control of the experimental apparatus, combined with the existence of microscopic theories that are computationally tractable with various degrees of approximation.

At the simplest level, atoms in an optical lattice are described by Bloch waves familiar from the description of electrons in periodic condensed matter systems. At sufficiently large densities the interatomic interactions result in a rich range of nonlinear phenomena. Notably, the quantum phase transition from a superfluid to a Mott-insulator [5, 21] and generation of bright gap solitons [12] have been observed. When the condensate is moving relative to the lattice, the nonlinearity can induce a dynamical (or modulational) instability that leads to an observed thermalization of the condensate [13, 14, 15, 16, 17, 18, 19, 20].

There has been a large amount of theoretical work devoted to instabilities in optical lattices [19, 20, 22, 23, 24, 25, 26, 27, 28, 29, 30, 31, 32, 33, 34, 37, 38, 39, 40, 41, 42]. Two types of instabilities are known to occur: dynamical and energetic. Energetic (or Landau) instabilities exist when the superfluid or condensate is not at a local minimum of energy, and can deplete the condensate via dissipative processes such as interactions with a thermal cloud [32, 33]. Dynamical instabilities manifest as an exponential growth of certain modes and are related

to the process of parametric amplification. A dynamical instability will rapidly deplete even a pure, isolated condensate. This process will often be chaotic and cause period doubling [28, 43], turbulence and vortex formation [27], and a loss of coherence of the condensate. A dynamically unstable BEC will eventually thermalize to a higher temperature.

On the other hand, the parametric amplification that causes the dynamical instability can be used to generate interesting states of the condensate. Hilligsøe and Mølmer [44, 45] have shown that momentum and energy can be conserved in non-trivial collisions between atoms in a 1D system with a periodic potential. This is in contrast to free space, where such collisions are energetically forbidden. This process is analogous to phase-matching in optical parametric amplification, and has been observed with a Bose-Einstein condensate both spontaneously and with seeding by Campbell *et al.* [46]. Related parametric amplification processes have been observed in systems with modulated lattices [43]. Parametric generation creates sub-Poissonian number correlations and quadrature entanglement between different modes in optical experiments, and is expected to do the same for atomic systems [47].

To quantitatively simulate dynamical instabilities in a BEC it is necessary to use beyond-mean-field method for quantum dynamics. In this paper we will be making use of the truncated Wigner method [48, 49, 50]. This method has successfully been previously applied to condensates in optical lattices by a number of authors. Firstly, Polkovnikov and Wang studied the unstable dynamics of an condensate offset in a combined optical lattice plus harmonic potential [34], which lead to damped Bloch oscillations. Isella and Ruostekoski investigated the dynamics of a trapped condensate as an optical

lattice was switched on and found number squeezing in experiments is limited because adiabatic ramping takes a very long time [35, 36]. In another work the same authors found that quantum fluctuations cause dissipation via the dynamical instability in the system [37]. Katz *et al.* investigated scattering due to the dynamical instability at the band-edge of an optical lattice using a 2D model [20]. They observe that the structure of the scattering halo can deviate strongly from the s-wave halo in free space.

In this paper we report on experiments where we observe rapid thermalization of a Bose-Einstein condensate at the band-edge of a one-dimensional optical lattice. We then model our system using a mean-field approach, but demonstrate that we are unable to accurately describe the dynamics of our system with the Gross-Pitaevskii equation. We then employ the truncated Wigner method to simulate beyond mean-field quantum dynamics of the system starting from a coherent condensate at zero temperature. In our simulations, we observe dynamical instabilities that lead to heating in qualitative agreement with the experimental results. We attempt quantitative modeling of the experiments and compare our numerical results to the experimental data.

This paper is organized as follows. In Sec. II we describe our experiments where a BEC is loaded into a 1D optical lattice and our observations of the resulting dynamics. Section III models the experiments using the mean-field Gross-Pitaevskii equation, and describes the physics that can be captured by this approach. In Sec. IV we describe the nature of the dynamical instability in various parameter regimes including those relevant to our experiments. We introduce our quantum model of the system in Sec. V, and discuss its advantages and limitations. Section VI describes our numerical results and studies the instabilities present for systems of different dimensionality. In Sec. VII we discuss important experimental considerations that have not been implemented in our simulations and use our results to develop a quantitative estimate of the heating rates that are observed in the experiments, before concluding in Sec. VIII.

## II. EXPERIMENTAL RESULTS

### A. Experimental Set-Up

Our experimental set-up has previously been described by Mellish *et al.* [11]. Briefly, we use a double magnetic-optical trap set-up to collect and pre-cool  $^{87}\text{Rb}$  atoms. The sample is then loaded into a QUIC magnetic trap, from which evaporative cooling results in a Bose-Einstein condensate of approximately  $1 \times 10^5$  atoms in the  $|F=2, m_F=2\rangle$  hyperfine ground state with a condensate fraction of approximately 80%. The peak density in the magnetic trap is  $\sim 1.7 \times 10^{20} \text{ m}^{-3}$  with an axial trap angular frequency of  $\omega_x \approx 2\pi \times 14.6 \text{ Hz}$  and a radial angular frequency of  $\omega_y = \omega_z \approx 2\pi \times 179 \text{ Hz}$ .

In our experiments a weak moving optical lattice is suddenly applied to the condensate at an angle of  $63 \pm 3^\circ$  to the weak axis of the trap. The lattice potential is generated from a single laser of wavelength 780 nm detuned 4.49 GHz from atomic resonance to minimize spontaneous emission. In the lab frame, the two lasers of wave-number  $|\mathbf{k}_L| = k_L \approx 2\pi/(780 \text{ nm})$  and angular frequency difference  $\delta$  produce a moving sinusoidal potential

$$V_L(\mathbf{r}, t) = \frac{V_0}{2} \cos(2\mathbf{k}_L \cdot \mathbf{r} - \delta t), \quad (1)$$

where  $V_0$  depends on the intensity of the lasers and the interaction with the atoms. For ease of analysis we define:

$$V_0 = s \frac{\hbar^2 k_L^2}{2m}, \quad (2)$$

where  $m$  is the mass of the atoms, and  $s$  characterizes the strength of the lattice. The frequency difference between the beams is chosen so that relative to the lattice the atoms are moving with a quasi-momentum corresponding to the Brillouin zone edge (the Bragg condition). In the frame of the lattice, the atoms are moving with momentum  $-\hbar\mathbf{k}_L$ .

### B. Bragg Scattering

We can gain a basic understanding of the system in the dilute, collisionless limit. The single-particle eigenfunctions of the Hamiltonian without the magnetic trap are the spatially periodic Bloch states that are superpositions of momentum components differing by  $2\hbar k_L$ . Diagonalizing this in the limit  $s \ll 1$  one finds the Bloch states at the edges of the two lowest bands are superpositions of the two momentum states  $|\pm k_L\rangle$  (in the frame of the lattice). Denoting the Bloch state with quasi-momentum  $\hbar q$  in the  $n$ th band by  $|q, n\rangle$ , we have the result:

$$\begin{aligned} |k_L, 1\rangle(t) &= \frac{|+k_L\rangle - |-k_L\rangle}{\sqrt{2}} e^{-i\omega_1 t} \\ |k_L, 2\rangle(t) &= \frac{|+k_L\rangle + |-k_L\rangle}{\sqrt{2}} e^{-i\omega_2 t}, \end{aligned} \quad (3)$$

and that  $\hbar\omega_2 - \hbar\omega_1 = V_0/2$ . This means that an atom suddenly placed in the lattice with definite momentum  $+k_L$  is in a superposition of the above modes, and furthermore the momentum will Rabi oscillate between  $\pm k_L$  at a frequency  $\omega_2 - \omega_1$  in a process rather similar to a Bloch oscillation.

By applying the lattice for an appropriate amount of time one can transfer any fraction of the condensate from one momentum state to the other (Bragg scattering). Alternatively, by phase shifting the optical lattice at the appropriate time one can non-adiabatically load a weakly-interacting condensate into an eigenstate of the lattice at either of the lowest two band edges, as described previously in Mellish *et al.* [11].

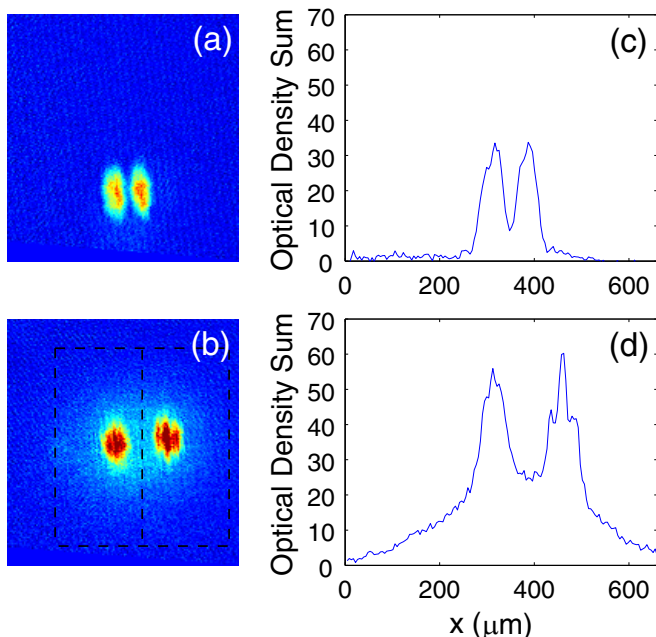


FIG. 1: Typical time-of-flight images of a condensate after it has been in an optical lattice at the Brillouin zone boundary (Rabi cycling). Atomic clouds to the right are the atoms that have been Bragg scattered (excited). (a) Collisionless regime,  $t = 280 \mu\text{s}$  (applied to freely expanding atoms 10 ms after being released from the trap), after 23 ms total time of flight. (b) Nonlinear regime,  $t = 240 \mu\text{s}$  (applied to trapped atoms) and 29 ms time of flight. The dashed boxes show typical regions of interest used for fitting the data. Also, the clouds in (b) are further apart and larger than those in (a) due to an additional 16 ms of expansion after the lattice is removed. (c) and (d) are  $x$ -axis profiles of the absorption images (a) and (b) respectively, summed along the vertical axis.

### C. Experiments in the Collisionless Regime

We present two sets of experiments in this paper. In the first, after creating the condensate we turn off the magnetic trap and allow the condensate to expand for 10 ms in order to reduce the effect of interactions. This allows for the dissipation of essentially all of the mean-field interaction energy. We then suddenly turn on and hold the optical lattice potential for a total time  $t$ , followed by a further 13 ms expansion (totalling 23 ms since being released from the trap) before imaging. In the frame of the lattice, the condensate begins with momentum  $-\hbar k_L$ , and as expected we find that the condensate undergoes Rabi oscillations between  $\pm\hbar k_L$  momentum in this frame.

An absorption image after a lattice evolution time of  $t = 280 \mu\text{s}$  is provided in Fig. 1(a), where we see roughly equal populations in the two momentum modes. To find the populations in each mode, we perform a bimodal fit to the data at momentum  $+\hbar k_0$  and  $-\hbar k_0$ . In the region surrounding each momentum state we fit a Gaussian distribution for the thermal component and an inverted

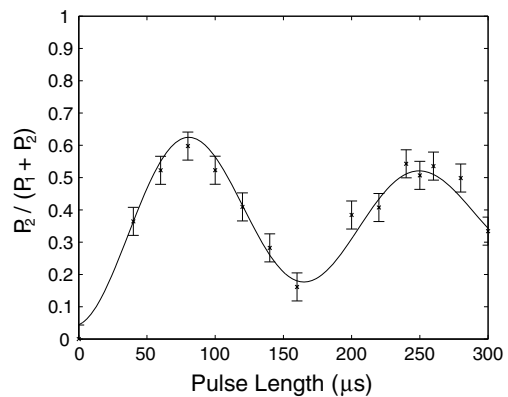


FIG. 2: Fraction of the population that has momentum  $> 0$  in frame of the lattice (i.e. the Bragg scattered atoms) as a function of the amount of time the lattice is applied after 10 ms of free expansion.

parabola for the condensate. We denote the condensed population in the region of interest surrounding the original condensate as  $N_1$  and that in the second region of interest as  $N_2$ . Similarly we define the total population (condensed and non-condensed) in each region as  $P_1$  and  $P_2$ .

The oscillation between the momentum states is plotted in Fig. 2. From the frequency of this Rabi oscillation ( $5.9 \pm 0.6 \text{ kHz}$ ) we estimate the strength of our optical lattice, and find that  $s \approx 3.1 \pm 0.3$ . The Rabi oscillation is damped due to the finite momentum width of the wave function of the initial condensate. An exponentially decaying sinusoid is fitted to the data in Fig. 2 for which the damping time is  $400 \pm 200 \mu\text{s}$ . We investigate the damping due to dephasing theoretically in Sec. III B.

### D. Experiments in the Nonlinear Regime

In the second set of experiments the optical lattice is suddenly turned on while the condensate is still confined in the magnetic potential. The BEC evolves in the combined potential for a time  $t$  before the lattice, and then the magnetic trap, are both rapidly switched off. An absorption image is then taken after 29 ms of free expansion to observe the resulting momentum distribution. For the short range of times  $t$  in these experiments there is essentially no change in the atomic density during the evolution in the trap, however as can be seen in Fig. 1 the momentum distribution undergoes significant evolution. The broad momentum distribution indicates that atoms have been scattered to a variety of different momentum states. The major difference between these experiments and those described in Sec. II C is that the density is much greater while the optical lattice is applied, suggesting that this effect is caused by nonlinear processes.

We observe that a fraction of the atoms still undergo Rabi oscillation between the  $\pm\hbar k_L$  momentum modes.

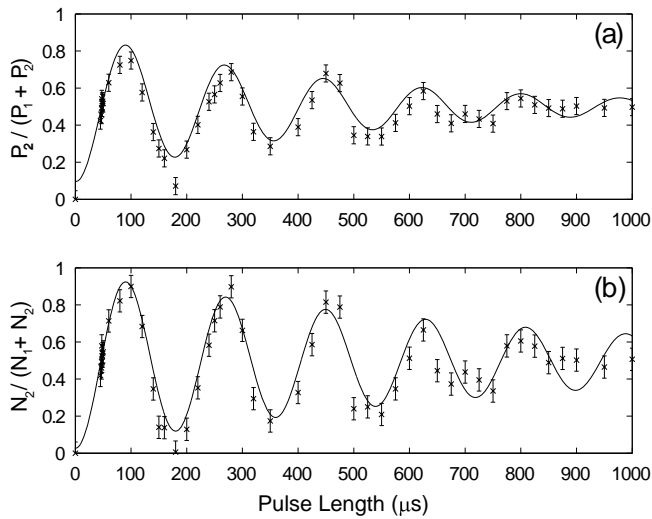


FIG. 3: In (a) we plot the fraction of the total population that has been Bragg scattered as a function of the time the lattice is switched on when the atoms are inside the trap. In (b) we plot the fraction of the condensed atoms, found with a Gaussian fitting procedure, that have been Bragg scattered.

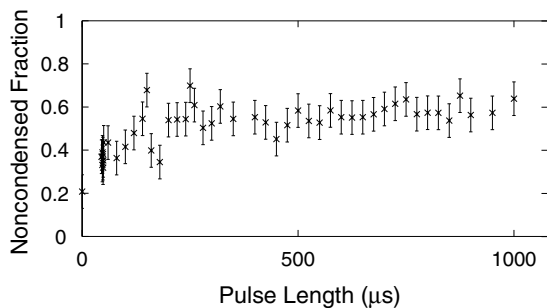


FIG. 4: The non-condensed fraction is plotted as a function of the time the lattice is left on inside the trap.

In Fig. 3 we plot the oscillating populations of both the entire sample, and the condensed modes found by the bimodal fitting procedure, finding qualitative agreement with previous results in [19]. By fitting an exponentially decaying sinusoid, we observe a damping time of  $\tau_P = 450 \pm 80 \mu\text{s}$  for the entire sample. However, we find that the condensed modes oscillate for much longer with a damping time of  $\tau_N = 800 \pm 100 \mu\text{s}$ . The fact that this is longer than the damping time measured in the experiments in the collisionless regime is due to the reduced momentum width of the condensate inside the trap. In the expansion process the interaction energy of the condensate is converted to kinetic energy, resulting in a broader momentum distribution.

The fraction of non-condensed atoms as a function of the evolution time in the lattice is plotted in Fig. 4. One can see that the non-condensed fraction grows rapidly until it saturates at slightly above 50%. This rapid generation of the thermal component has been termed ‘anomalous heating’ by other authors [51]. Understanding this

apparently nonlinear process is the main goal of this paper.

### III. MEAN FIELD DYNAMICS

In this section we turn to a common tool of choice for modelling BEC experiments near  $T = 0$ : the Gross-Pitaevskii equation (GPE). The mean-field dynamics described by the GPE have often proven to be in excellent agreement with observations in a number of experiments [52].

#### A. The Gross-Pitaevskii Model

The time-dependent Gross-Pitaevskii equation for the evolution of the macroscopic wave function  $\psi(\mathbf{r}, t)$  of a BEC is

$$i\hbar \frac{\partial \psi(\mathbf{r})}{\partial t} = -\frac{\hbar^2}{2m} \nabla^2 \psi(\mathbf{r}) + V(\mathbf{r})\psi(\mathbf{r}) + U_0 |\psi(\mathbf{r})|^2 \psi(\mathbf{r}). \quad (4)$$

The characteristic strength of atomic interactions is  $U_0 = 4\pi\hbar^2 a_s/m$  where  $a_s$  is the s-wave scattering length which for  $^{87}\text{Rb}$  we take to be  $a_s = 100$  Bohr radii. The external potential  $V(\mathbf{r}, t)$  in the experiment is

$$V(\mathbf{r}, t) = \frac{m}{2} (\omega_x^2 x^2 + \omega_y^2 y^2 + \omega_z^2 z^2) + V_L(\mathbf{r}, t), \quad (5)$$

which is the sum of the parabolic magnetic potential of the trap and the sinusoidal optical potential from Eq. (1). The trap frequencies are those measured by the experiment:  $(\omega_x, \omega_y, \omega_z) = 2\pi \times (14.6, 179, 179)$  Hz.

Our simulations begin with  $10^5$  atoms in the Thomas-Fermi ground state, which has a peak density of  $n_0 \approx 1.69 \times 10^{20} \text{ m}^{-3}$ .

#### B. Linear Regime

The density of the system decreases rapidly after release from the trap, and so interactions between the particles become negligible in the experiments where the lattice is applied after 10 ms of free expansion. A simple one-body theory can therefore be applied to this system [taking  $U_0 |\psi|^2 = 0$  in Eq. (4)]. We will now derive an analytic approximation to the form of the damped oscillations. The Rabi frequency of oscillation of an atom is dependent on its initial momentum, and the momentum width of the condensate gives a spread of Rabi frequencies whose sum results in the damping of the full oscillations.

It is worth noting that the dimensionality of the problem can be reduced. Any momentum orthogonal to the lattice does not affect the oscillation frequency, and therefore is not a part of our dephasing analysis. Thus, we only need to look at the distribution of momenta in the lattice direction. The distribution is a result of the initial

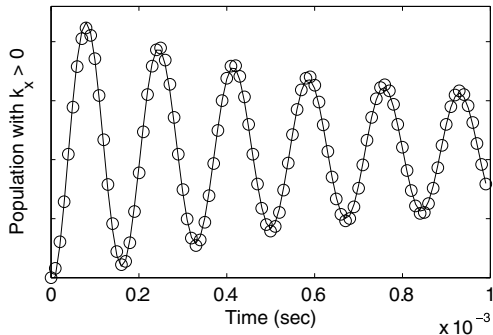


FIG. 5: Comparison of our analytic estimate for the damped Rabi oscillations due to dephasing of a non-interacting condensate with a full numerical calculation. In both cases we have assumed a Gaussian distribution of initial momenta which dephase with each other. Circles represent data from numerical simulations, and the line is the analytic result in Equation 10.

momentum within the trap plus the released interaction energy and would be difficult to calculate precisely. We introduce a few approximations below.

To simplify analysis, our initial distribution was taken to be Gaussian

$$P(k) \propto \exp\left(-\frac{(k - k_L)^2}{2\sigma_k^2}\right), \quad (6)$$

where almost all of our kinetic energy comes from the released interaction energy  $U_{\text{int}} = \frac{2}{7}U_0n_0$ . Due to the high aspect ratio of the trap, almost all this energy is distributed equally in the two tightly-trapped dimensions. Given that the lattice is at angle  $\theta \approx 63^\circ$  to the weak axis of the trap, the conservation of energy requires that

$$\frac{\hbar^2\sigma_k^2}{2m} = \frac{\sin^2\theta}{7}U_0n_0. \quad (7)$$

This results in an predicted  $\sigma_k \approx 1.23 \times 10^6 \text{ m}^{-1}$ .

We will now analyze the dynamics that these modes will undergo. In a periodic potential, the eigenstates are superpositions of momentum states corresponding to the same quasi-momentum (i.e.  $\hbar k \pm 2n\hbar k_L$  where  $n$  is an integer). We can then find the rate of oscillation between two modes of the same quasi-momentum. At the band edge, we assume the eigenstates to be superpositions of only the momentum modes  $|\pm k_L\rangle$ . The energy difference  $\hbar\omega_0$  between the two states at the band-edge

$$\hbar\omega_0 = \frac{\hbar^2 k_L^2}{2m} \frac{s}{2}, \quad (8)$$

is accurate for small values of  $s$ , and has a 1% error (compared to direct diagonalization) for the value of  $s = 3.1$  used in these simulations and experiments. The Rabi frequency of the oscillation is  $\omega_0$ .

Next we will find how the oscillation frequency varies with the quasi-momentum. We will assume that the

eigenstates are superpositions of the modes  $|\Delta k + k_L\rangle$  and  $|\Delta k - k_L\rangle$  only. In this basis, we see the energy difference between the upper and lower states is (to second order in  $\Delta k$ ):

$$\hbar\omega \approx \hbar\omega_0 + \frac{8\hbar^2(\Delta k)^2}{sm}. \quad (9)$$

We can now use this dispersion relation, and the initial conditions of Eq. (6) to find the distribution as a function of  $\omega$ . Performing the Fourier transform yields the population of the negative momentum modes in time

$$N^{(-)} = N_0^{(-)} \left(1 - \frac{\cos[\omega_0 t + \arctan(t/\tau)/2]}{(1 + t^2/\tau^2)^{1/4}}\right), \quad (10)$$

where  $\tau = sm/16\hbar\sigma_k^2 \approx 174 \mu\text{s}$ . Note that the functional form of this decay is much slower than exponential, and goes as  $t^{-1/2}$  for  $t \gg \tau$ . To give an idea of the validity of the approximation in Eq. (9), we also performed a numerical simulation using the linear Schrödinger equation and the same Gaussian initial conditions. Fig. 5 demonstrates agreement between the analytical estimate and the numerical results.

To compare with the experiment, we fitted an exponential decaying sinusoid to the first 300  $\mu\text{s}$  of data in Fig. 5, yielding a decay time of 954  $\mu\text{s}$ , compared to a measured time of  $400 \pm 200 \mu\text{s}$ .

There are several reasons that might explain the discrepancy between the theoretical and experimental results. Firstly, the initial condition of the condensate may be quite different from Gaussian due to nonlinear and finite temperature effects. Condensates may begin with a small, random center-of-mass momentum, giving an apparent dephasing effect shot-to-shot. Alternatively, the condensate may have larger momentum width due to heating or other effects.

We have estimated the momentum width necessary for an exponentially decaying fit to the derived expression to return the same decay time as the experiment. This yields  $\sigma_k \approx 1.75 \times 10^6 \text{ m}^{-1}$ , which is 41% greater than our prediction. Approximately twice the predicted initial kinetic energy is required to explain the experimental results.

### C. Nonlinear Regime

We now apply the Gross-Pitaevskii theory to simulate the condensate dynamics in the combined magnetic and optical potential. We perform a full 3D calculation directly matching the experimental parameters described earlier. The initial condition for the calculation is generated via imaginary time evolution to find the ground state containing approximately  $1 \times 10^5$  atoms.

In Fig. 6 we display the momentum distribution after the lattice applied to the trapped atoms for (a) 0.5 ms and (b) 1 ms respectively. The broad, thermal features observed in the experiment are not apparent in the

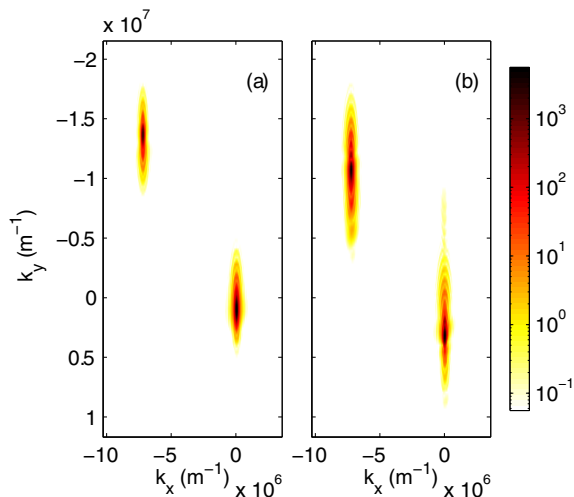


FIG. 6: Population per mode in momentum space is shown (a) 0.5 ms and (b) 1 ms after the lattice is applied in a three-dimensional GPE simulation. The  $x$ -axis is the weak trapping axis. The condensate is visible at zero momentum and  $2\hbar k_0$ , but no thermal features are visible. Note the “camera” angle is different to the experiment and a logarithmic scale is used.

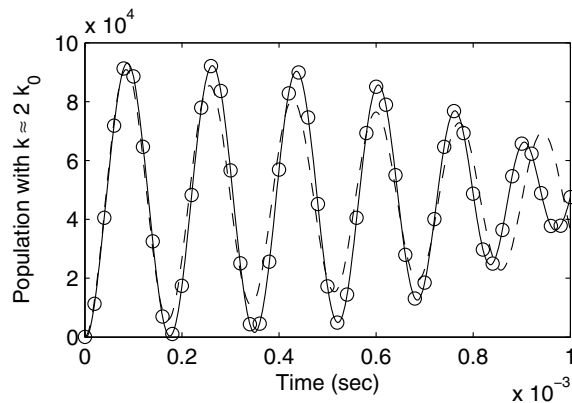


FIG. 7: Total population with positive momentum in the lattice frame for a full 3D GPE calculation corresponding to the in trap experiment showing damped Rabi oscillations. A cubic spline (solid line, to guide the eye) and an exponential decay (dashed line) were fitted to the simulation results (circles). The exponential decay constant is  $\tau = 1.3$  ms.

simulation. However, small ripples in the condensate momentum densities are indications of linear dephasing. We observe that the momentum distribution of the condensate modes broadens slowly in time. The center of mass of the two condensates also evolve in time as the condensates climb the walls of the trapping potential.

In Fig. 7 we plot the populations with positive velocity relative to the moving lattice. An exponentially decaying sinusoidal fit results in a decay time of 1.3 ms. We note that the exponential decay fits poorly to the numerical results. Qualitatively, some features of the shape of the decay envelope matches more closely to that derived in Eq. (10). In particular, the decay is slower than expo-

ponential for short times and there is a notable phase shift (or a change in frequency) reminiscent of the second term inside the cosine of Eq. (10).

In the experiment we were able to separate the evolution of the condensed atoms from the non-condensed, as shown in Fig. 3 (b). The damping of the condensate oscillations is at least partly caused by the linear dephasing. Linear dephasing is present in this simulation, and should be comparable to that of the experiment. However, we see that the numerical result of 1.3 ms is slower than the experimental fit of 800  $\mu$ s. More favorable agreement was found in Ref. [19] where the authors applied a similar comparison with their experiment.

The Gross-Pitaevskii simulation did not generate the thermal features found in the experiment. However, semiclassical theory can explain the occurrence of thermalization by the existence of dynamical instabilities, as shall be discussed below.

#### D. Dynamical Instabilities

The Gross-Pitaevskii equation is a non-linear equation that is known to exhibit dynamical instabilities.

Stationary states of the GPE may, under certain circumstances, be unstable points of equilibrium. That is, perturbations to the state may grow exponentially in time. Eventually, for any realistic initial condition the growing perturbations will alter the state significantly.

The presence of dynamical instabilities can be detected by linearizing the GPE about the stationary state, or equivalently by solving the Bogoliubov-de Gennes equations. Quasi-particle modes with imaginary eigenvalues are those that undergo exponential growth and are dynamically unstable. Alternatively, modes can have negative eigenvalues indicating energetic (Landau or thermodynamic) instabilities.

There has been significant theoretical and experimental research into the presence of dynamical instabilities in condensates in optical lattices [13, 14, 15, 16, 17, 22, 23, 24, 25, 26, 27, 28, 29, 30, 31, 32, 33, 34, 37, 38, 39]. What is certain is that dynamical instabilities cause the thermalization of the condensate when placed at the band edge of an optical lattice at high enough densities.

We will not repeat previous work, but simply point out that quantitatively accurate simulations of the regime in this experiment have not been performed as far as we are aware. This regime involves a condensate at the band edge of a relatively weak 1D optical lattice, where transverse excitations play an important role (as discussed in Sec. IV). The reason for this is the lack of spontaneous processes in deterministic, semiclassical simulations. Accurate quantum dynamics in other regimes has been performed in [34, 37, 38].

The exponential growth of quasi-particle modes is a result of Bose enhanced (stimulated) processes. However, even with zero initial population in the quasi-particle mode there is the chance of spontaneous scattering into

that mode. These spontaneous processes are very important when determining the subsequent dynamics of the condensate. In fact, in some regimes the spontaneous processes dominate over the stimulated ones, as discussed in the next section.

#### IV. REGIMES OF DYNAMICAL INSTABILITY IN ONE-DIMENSIONAL LATTICES

In this section we discuss the effect of dynamical instability on the condensate when one considers the spontaneous processes that may occur.

The character of the dynamical instability in a lattice is dependent on many factors, including the interaction strength, the number of particles, the strength of the lattice and the dimensionality of the system. The role of excitations in the directions transverse to the lattice was studied thoroughly in Ref. [30]. They showed that, for small enough  $s$ , that there was a significant difference in the stability diagram for 1D and 3D models.

In our system, where  $s \approx 3.1$ , we would expect transverse excitations to be important features of the dynamical instability. Our eventual goal is to quantitatively describe the dynamics of the condensate and so eventually must perform a full three-dimensional analysis. However, we will first discuss the dynamical instability in systems of lower dimensionality.

For quasi-one-dimensional systems, one can expect a narrow band of modes for which collisions are both resonant (i.e. conserve energy) and conserve momentum modulo  $2\hbar k_L$  (i.e. quasi-momentum in the lattice). These are the modes which will undergo rapid exponential growth. For the case of a pure condensate, the process is initiated by spontaneous collisions between condensate particles. Then, as the number of particles in the resonant modes grow, Bose-enhancement of the scattering process causes parametric amplification. The timescale for this growth to become significant will depend on the initial rate of spontaneous scattering, and so should be included in any model which attempts to quantitatively model dynamics. At later times, secondary collisions between atoms will lead to thermalization of the system.

For higher-dimensional systems there will be a much larger volume in phase-space where collisions are close to resonance, most of which incorporate an excitation transverse to the lattice dimension. In this case the total rate of condensate depletion by spontaneous scattering is greatly increased. However, as there are many more modes the effect of Bose-enhancement is significantly reduced. For some systems the number in each mode may not grow much at all before the condensate is entirely depleted. In this situation the parametric nature of the dynamical instability will be washed out by spontaneous processes. Note that secondary collisions would be expected in these systems too, which will lead to thermalization. Thus, in systems of any dimensionality one could

expect to observe rapid thermalization of the condensate.

As an example, consider a system in the limit of a weak lattice (small  $s$ ). In this case the dispersion spectrum is not modified significantly from the free particle case. However, oscillations in momentum due to the lattice are expected to occur. At the band-edge one would expect Rabi oscillations between modes with momentum  $\pm\hbar k_L$ . Assuming that the dispersion spectrum is not significantly different to free space, one would expect resonant collisions between the modes with momentum  $\pm\hbar k_L$  into a spherical shell of momentum with modulus  $\hbar k_L$  [53, 54, 55]. We can derive the spontaneous collision rate using Fermi's second golden rule.

For a system with a total of  $N \approx 10^5$  particles in a volume  $V \approx 10^{-15} \text{ m}^3$  the spontaneous scattering rate is:

$$\frac{dN}{dt} = \frac{U_0^2 N^2 m |k_L|}{2\pi \hbar^3 V} \approx 4 \times 10^7 \text{ s}^{-1}, \quad (11)$$

where we have substituted values appropriate to our experiment. Thus, 10% of the condensate is lost in just 250  $\mu\text{s}$  by spontaneous collisions.

Of course, this value will not be accurate for  $s \approx 3$ , and does not take into account that the atomic populations are oscillating between the two momentum states or the effect of Bose-enhancement. This does however highlight that rapid thermalization does not require parametric growth in dynamically unstable 3D systems, but could be simply provided by a sufficiently large density of states at resonance.

#### V. QUANTUM MODEL

The second-quantized Hamiltonian for an ultra-cold Bose gas is:

$$\hat{H} = \int d^3\mathbf{r} \left[ \hat{\psi}^\dagger(\mathbf{r}) \left( -\frac{\hbar^2}{2m} \nabla^2 + V(\mathbf{r}, t) \right) \hat{\psi}(\mathbf{r}) + \frac{U_0}{2} \hat{\psi}^\dagger(\mathbf{r}) \hat{\psi}^\dagger(\mathbf{r}) \hat{\psi}(\mathbf{r}) \hat{\psi}(\mathbf{r}) \right], \quad (12)$$

where the field operator  $\hat{\psi}(\mathbf{r})$  annihilates an atom of mass  $m$  at position  $\mathbf{r}$  and obeys the commutation relation  $[\hat{\psi}^\dagger(\mathbf{r}), \hat{\psi}(\mathbf{r}')] = \delta^3(\mathbf{r} - \mathbf{r}')$ .

It is not possible to analytically solve for the evolution of a Bose gas system directly from the Hamiltonian in Eq. (12). Analytical approaches always involve approximations, and often linearize the quantum fluctuations about the mean-field as in the Bogoliubov approach. Numerical solutions are possible with the exact Positive-P method, but quickly become intractable with sampling problems in many situations [48]. The approximate Gross-Pitaevskii equation (GPE) is straightforward to solve, but fails to account for any spontaneous effects that are important for the problem we are considering.

In this paper we implement the truncated Wigner phase-space method for the system dynamics. This is

an approximate method that goes beyond the GPE by including both spontaneous processes and the dynamics of non-condensate modes.

### A. The Truncated Wigner Method

We will now briefly explain the origin and use of the truncated Wigner method. This was used in the context of squeezing of solitons in optical fibres by Carter and Drummond [56], and was first applied to Bose gases by Steel *et al.* [48]. An equation of motion for the Wigner function can be obtained from the Hamiltonian Eq. (12) by deriving the master equation for the system followed by the appropriate transformation of the density operator. However, for a system with  $n$  modes the Wigner function is  $2n$ -dimensional and it is impractical to solve such an equation directly.

However, truncating the third-order derivatives in the equation of motion for the Wigner function results in a Fokker-Planck equation, which can then be simulated using stochastic methods [49, 57]. The omission of the higher order terms has previously been justified when there are more particles than modes in a calculation and the simulated times are short [54, 55, 58]. The equation of motion for the stochastic trajectories is simply the usual Gross-Pitaevskii equation, although the initial conditions for the field are sampled stochastically from the appropriate Wigner distribution. A large number of trajectories must be calculated, which are then sampled to obtained expectation values of symmetrically-ordered quantum field operators.

As an example, the ensemble average  $\overline{\psi^*\psi}$  is equal to the expectation of the symmetric ordering of the number operator, or  $\langle\hat{\psi}^\dagger\hat{\psi} + \hat{\psi}\hat{\psi}^\dagger\rangle/2$ . Therefore, the average number of particles in a mode is  $\langle\hat{\psi}^\dagger\hat{\psi}\rangle = \overline{\psi^*\psi} - 1/2$ . For more details on the truncated Wigner and other phase space methods see [48, 49, 50].

Because of the nonzero width of the Wigner distribution, every vacuum mode begins with uncorrelated Gaussian noise, normalized to an average of half a particle per mode. This provides the seeding needed for the equation of motion (the GPE) to allow scattering events into these modes. Furthermore, the rate of scattering corresponds to that of the expected spontaneous processes.

Allowing such spontaneous processes is essential to accurately model systems exhibiting instability. Unstable dynamical solutions of the GPE do not correspond accurately to quantum mechanics. Such states would eventually be altered by spontaneous processes and are therefore not equilibrium states. The truncated Wigner approach unambiguously allows both dynamical instabilities and Landau instabilities to manifest. Additionally, a background thermal gas can be included in the initial condition to allow dissipation via the Landau instability. The importance of the two instabilities has been a point of discussion in the past [13].

The disadvantage of the truncated Wigner method is

the accuracy of its fundamental approximation is difficult to quantify. However, some work has been done which demonstrates its validity regimes [55, 58, 59, 60, 61]. Some of these works have concluded that the major requirement for accuracy is that the number of modes must be much smaller than the number of real particles [58, 59]. If this is not the case, then the “vacuum noise” in the initial condition can no longer be considered a perturbation. The vacuum fluctuations will begin to interact as if they are real particles, and unrealistic effects such as negative expectation value for population become prolific [59].

The method in [60, 61] allows one to check the validity of the truncated Wigner approximation at the expense of significant extra computation. In this paper, however, we instead choose to work in the regime where there are more particles than simulated modes.

Unfortunately, this is not the case for the full 3D experimental parameters. Including the trap and the optical lattice whilst simultaneously avoiding numerical aliasing due to the nonlinearity requires of order  $10^6$  modes to represent  $1 \times 10^5$  atoms. Our calculations in this regime clearly display unphysical behavior similar to those found in [59]. In particular, we observe large areas of negative population at high momentum modes, and a corresponding clustering of the vacuum noise at small momentum which swamps the condensate. The condensate is rapidly depleted as it scatters off these unphysical particles.

To proceed we must make a further simplification by neglecting the trapping potential, and instead modeling a homogeneous system with a similar density to the experiment. By doing so we expect to capture the most important physics, as the timescale that the thermalization manifests is much shorter than the inverse trapping frequencies, so that whilst the optical lattice is on the atoms will be essentially stationary and the density constant. The most important effect of the trap in the experiment is to maintain the high density so that collisions may occur. This model requires fewer modes to simulate the dynamics, and therefore the truncated Wigner method is expected to be more accurate.

In the next section we describe the details and present the results from our truncated Wigner simulations. We point out in advance that while these calculations will model the spontaneous scattering in this system, the homogeneous calculations will not capture the linear dephasing of the Rabi oscillations in the experiment as the condensate begins in a single momentum state. We will consider this further in Sec. VII.

## VI. TRUNCATED WIGNER SIMULATIONS

In the experiment the initial inhomogeneous condensate wave function spreads over about 27 wells of optical lattice potential. We use a total population of  $10^5$  atoms and choose to use a density of  $n_0 = 10^{20} \text{ m}^{-3}$ , roughly corresponding to the average density within the trap



rather than the peak density. We have implemented a rectangular grid with periodic boundary conditions for our simulation space, with dimensions  $L_x \times L_y \times L_z$ . The lattice is parallel to the long axis of the space, with spacing 390 nm, extending over 32 wells, making  $L_x = 12.48 \mu\text{m}$ . It follows that  $L_y = L_z \approx 8.95 \mu\text{m}$ . Note that this geometry is slightly different to that of the extended condensate at a  $63^\circ$  angle to the lattice.

We begin with a homogeneous cloud moving at the Bragg condition with momentum of  $\hbar k_L$  in the direction of the stationary lattice. The nonlinearity and strength of the lattice are the same as used previously. Care was taken to ensure numerical accuracy, and a projection operator that prevents numerical aliasing [62, 63, 64] was employed.

In the following subsections we present our results of the truncated Wigner method used to simulate the experiment using 1D, 2D and 3D models. This was done for two reasons. The first was to demonstrate the different regimes discussed in Sec. IV. Secondly, the truncated Wigner method will be very reliable in the 1D and 2D models where the number of modes is much smaller than the number of particles.

To compare the simulations at different densities we have ensured that the nonlinearity has scaled correctly. In 1D, the nonlinearity is  $U_0/(L_y L_z)$  and in 2D it is  $U_0/L_z$ .

The one-dimensional results in Sec. VIA clearly show the dynamical instability and the parametric gain of the resonant modes. The two-dimensional simulations in Sec. VIB allow us to clearly visualize the transverse excitations, as was achieved previously in [20]. We also analyze the coherence and statistics of the field in 2D where statistical errors are more manageable than the 3D situation, as more trajectories can be computed for the same amount of CPU time. Finally, in Sec. VIC we show the results of the complete three-dimensional simulation that exhibits strong spontaneous scattering and make a comparison to the experimental results.

### A. One Dimension

We first investigate the dynamical instability in one-dimension. Figure 8 shows results for a single trajectory, which in some sense can be considered to be analogous to what might be observed in a single experiment in the lab [55]. In real space, we observe spontaneous breaking of the translational symmetry of the lattice brought about by the dynamical instability. The high-density features correspond to generation of bright-gap solitons. These solitons are known to be generated from states near the top of the ground band for condensates with repulsive interactions [23]. The momentum distribution broadens indicating spontaneous collisions between condensate atoms scattering atoms to other momentum modes.

The work of Hølligsøe and Mølmer [44, 45] predicts that collisions that conserve energy and momentum (i.e.

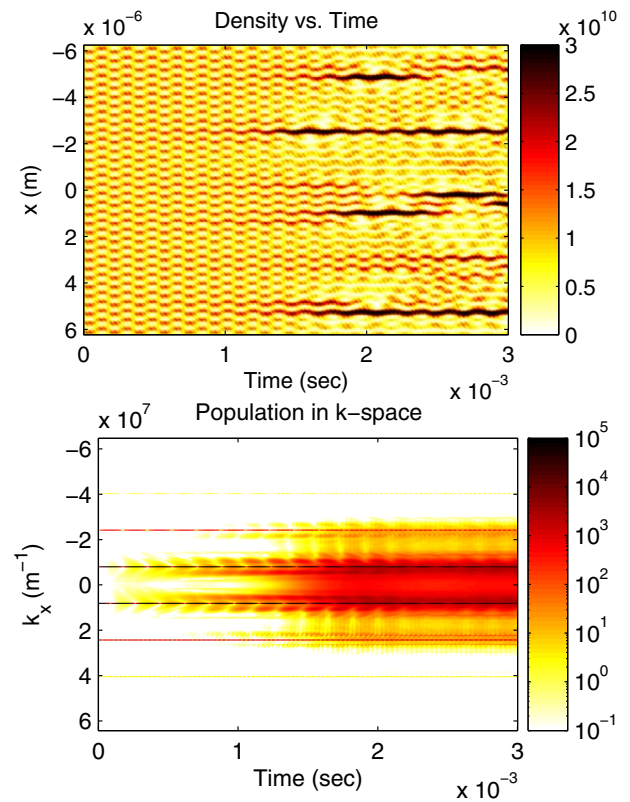


FIG. 8: (Color online) Top: Density of a 1D BEC moving in an optical lattice. We see spontaneous symmetry breaking of the BEC in a single trajectory simulation. The localized regions of high density are bright-gap solitons. Bottom: The same results are presented in momentum space, where symmetry breaking is characterized by mixing into a variety of different modes (note the logarithmic dependence of the density scale).

resonant collisions *in the eigenbasis of the lattice*) will experience parametric growth. If energy conservation is not quite satisfied for a particular mode then observe Rabi oscillations are expected that will hinder the exponential growth of parametric amplification. This is exactly what we observe in the simulation as the resonance condition is never precisely matched. This effect is demonstrated in Fig. 9, where population revival into the states  $\pm k_L$  can be seen. Also note that only about half the population is depleted from the two condensate modes – this corresponds to the half that are in the lowest band near the band-edge that generate a bright-gap soliton [23].

The experiments described in this paper indicate damping of the Rabi oscillations is due to dynamical instability. Our 1D simulations show damping occurring after a few milliseconds (see Fig. 9). Ensemble averages of 1000 trajectories have shown the spread of momentum states and the approach towards thermalization. It should be noted that phase coherence is also destroyed by the dynamical instability. This is an interesting example of decoherence under Hamiltonian evolution.

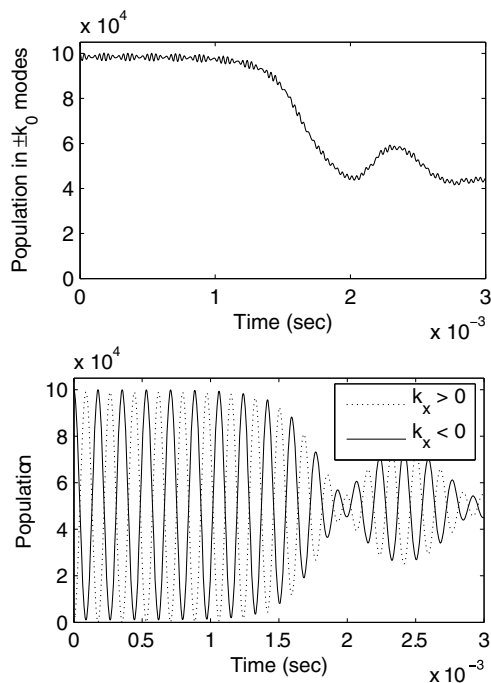


FIG. 9: Top: Sum of the population in the momentum modes  $\pm k_L$  of a 1D Bose gas plotted versus time. The small, rapid oscillations are due to the initial state mixing with higher band states in the Bloch basis. The atoms are depleted from the condensate mode, until a partial revival begins at  $\sim 2$ ms. This is due to Rabi oscillations of the not-quite resonant collisions. Bottom: Total populations of atoms with positive or negative momentum versus time. Damping of the Rabi oscillations is observed in the 1D simulations after 1.5ms, but then revive at the same time as the condensate as shown in the top figure. Both plots have used an ensemble of 1000 trajectories.

## B. Two Dimensions

### 1. Dynamical instability

As described above, the effect of dimensionality on the system varies according to the parameters of the experiment, and has been dealt with analytically in detail in [30]. In that treatment, the dynamical instability was studied as an exponential growth of Bogoliubov modes. A complete set of Bogoliubov modes includes excitations in the direction of the lattice (such as would be found in a 1D treatment), excitations in the directions perpendicular to the lattice, and excitations which are mixtures of both. For some parameter regimes, the perpendicular excitations are an important part of the dynamics.

The same is true in our homogeneous treatment. Collisions may be resonant into modes with non-zero components of momentum in the directions perpendicular to the lattice. This can be observed quite clearly in the results of our two dimensional simulations.

Figure 10 shows a comparison momentum distributions for four different initial conditions averaged over  $10^3$  tra-

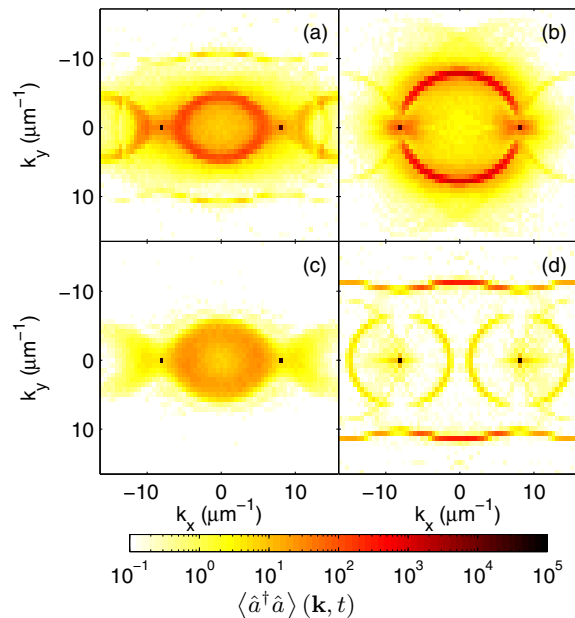


FIG. 10: (Color online) Populations in momentum space of a 2D simulation. (a) The condensate began in the lattice in the  $-k_L$  momentum state,  $t = 1.1$  ms. (b) The condensate began in a superposition of  $\pm k_L$  momentum in free-space for comparison with (a),  $t = 1.1$  ms. (c) The condensate began in the lowest band-edge of the lattice,  $t = 0.36$  ms. (d) The condensate began in the edge of the first excited band,  $t = 1.1$  ms. Movies of these simulations are available online at: <http://www.physics.uq.edu.au/people/ferris/>.

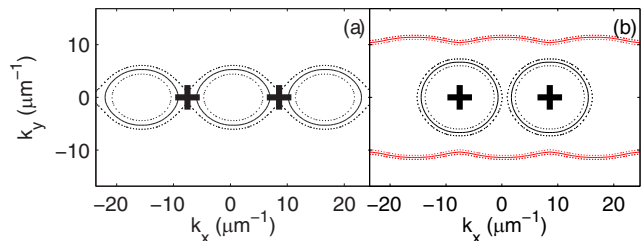


FIG. 11: (Color online) Plots of modes for which the resonance condition is satisfied. The dotted lines correspond to regions close to resonance, having an energy mismatch corresponding to a Rabi oscillation period of 1 ms. The large pluses represent the initial state of the BEC. (a) Two atoms colliding within the lowest band. (b) Two atoms begin in the second band-edge can collide to result in an atom in the lowest and second band (inner circles, black online) or two atoms in the lowest band (outer rings, red online).

jectories. In Fig. 10(a) the condensate begins in the  $+k_L$  momentum mode; in Fig. 10(b) we make a comparison to free space collisions between momentum modes  $\pm k_L$ . Figs. 10(c) and (d) begin with the atoms loaded into the ground and first excited band-edge states.

When the moving lattice is switched on such that the BEC is in the  $+k_L$  momentum state, we see complicated dynamics including Rabi oscillations and scattering into a variety of modes. A significant percentage of the atoms

have developed momentum in the direction perpendicular to the lattice, so we obviously can not characterize the system as quasi-1D.

We can understand the complicated dynamics by realizing that the initial condition is a superposition of momentum states as given in Eq. (3). Each of these states has a well-defined energy, and we can analyze which collisions will conserve energy and quasi-momentum (modulo  $2k_L$ ) in the Bloch basis. The system has been analyzed previously in a similar fashion [20, 45]. Katz *et al.* [20] provided comparisons with the results of truncated Wigner simulations and an experiment. They found, as we do, that the structure of the scattering halo differs significantly from the s-wave scattering sphere generated by condensate collisions in free space, due to the modified dispersion curve.

Two atoms initially at the edge of the first band can collide to produce atoms elsewhere in that Bloch band, but with additional kinetic energy in the transverse direction. We have calculated the resonance condition using the Hartree-Fock mean field method [65]. The values of momentum where this occurs is shown in Fig. 11(a) (*cf.* Fig. 10(c)). There are two possible outcomes for atoms colliding at the first excited band edge. Either one or both atoms can end up in the lowest band. Both of these cases are presented in Fig. 11(b) [*cf.* Fig. 10(d)]. Note that the resonance condition is sharper than in Fig 11(a), i.e. there is a smaller area of modes which have a final energy close to the resonance condition. This explains the results in Fig. 10, where the lowest band-edge initial condition exhibits significantly more scattering at short times than the second band-edge case.

## 2. Coherent and incoherent components

We have investigated the phase coherence of the atomic cloud as it undergoes thermalization. A Bose-Einstein condensate has off-diagonal, long-range order where there is a well-defined relative phase across the system. Any overall phase of the condensate results from spontaneous symmetry breaking, and the value of the global phase is undetermined.

Nevertheless, when employing classical field methods one typically begins with a coherent state, ascribing a global phase to the condensate at  $t = 0$  such that:

$$\left| \langle \hat{a}_0 \rangle \right|^2 = \langle \hat{a}_0^\dagger \hat{a}_0 \rangle, \quad (13)$$

where  $\hat{a}_0$  is the annihilation operator for the condensate mode. All observables of the closed system being simulated will return the same results if one averages over ensembles of random global phase, that is averaging  $\arg \langle \hat{a}_0 \rangle$  from 0 to  $2\pi$ .

The value of the phase of  $\langle \hat{a}_0 \rangle$  is only meaningful in respect to a second condensate of atoms. An interference experiment can resolve the phase relationship of two condensates. If one condensate undergoes heating

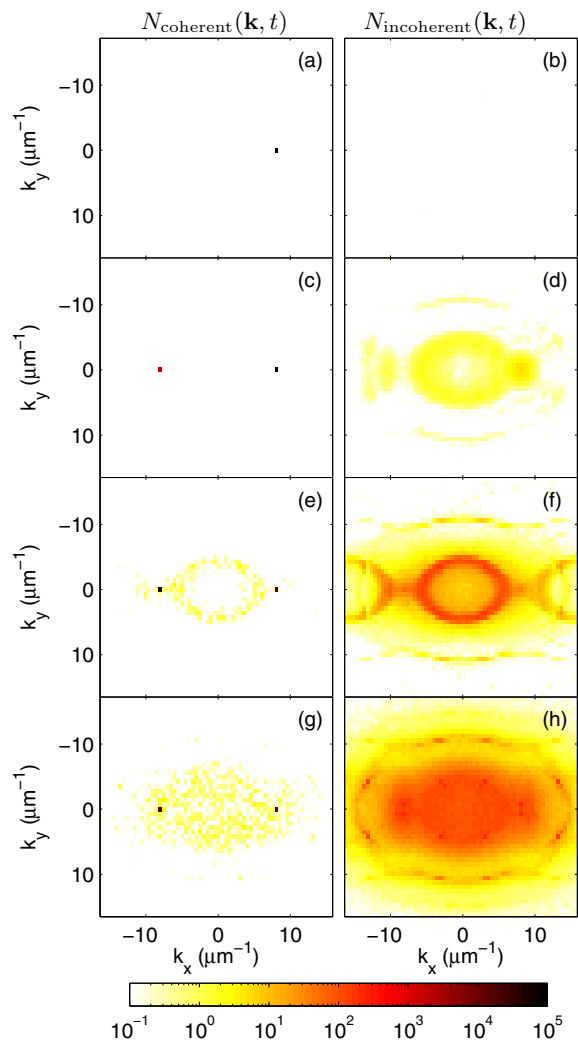


FIG. 12: (Color online) Coherent (a,c,e,g) and incoherent (b,d,f,h) populations in momentum space for the 2D simulation at times 0 (a,b), 0.56 ms (c,d), 1.1 ms (e,f), and 3 ms (g,h).

and becomes thermalized in an experiment, then that cloud of atoms will lose its coherence and not result in fringes in an interference experiment. For a thermal sample  $\langle \hat{a} \rangle = 0$ .

We define the *coherent* component of the cloud to be that with well-defined global phase

$$N_{\text{coherent}}(\mathbf{k}) = |\langle \hat{a}(\mathbf{k}) \rangle|^2. \quad (14)$$

The incoherent component is the remainder of the atoms

$$N_{\text{incoherent}}(\mathbf{k}) = \langle \hat{a}^\dagger(\mathbf{k}) \hat{a}(\mathbf{k}) \rangle - N_{\text{coherent}}(\mathbf{k}). \quad (15)$$

We plot the coherent and incoherent populations in Fig. 12 for the initial condition with the condensate in momentum state  $|+k_L\rangle$ . Coherent dynamics caused by the lattice drives the condensate into the modes with momentum  $\pm k_L, \pm 3k_L$ , etc. Only these modes contain any significant coherent population. Note the noise in

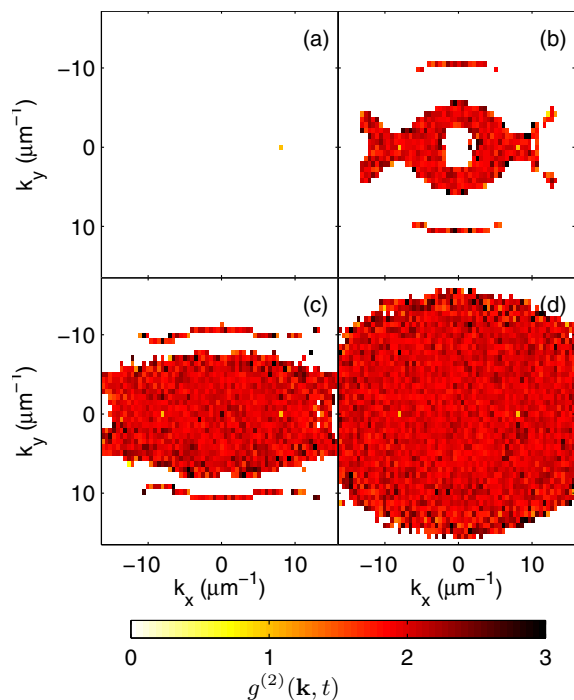


FIG. 13: (Color online) The normalized second order momentum-space correlation function  $g^{(2)}(\mathbf{k})$  is shown for the 2D simulation at times (a) 0 ms, (b) 0.56 ms, (c) 1.1 ms, and (d) 3.0 ms. Results are only shown for modes with average population greater than 1/2.

Fig. 12 (e,g) is a statistical artefact from averaging over only 1000 trajectories, and could be reduced with more CPU time.

The incoherent population is generated by spontaneous scattering into the non-condensate modes surrounding the condensate. At short times energy conserving collision from the two condensate modes dominates. At later times further scattering from the newly populated modes broadens the distribution and results in thermalization.

### 3. Local correlation functions

The normalized second-order local momentum-space correlation function is:

$$g^{(2)}(\mathbf{k}) = \frac{\langle \hat{a}^\dagger(\mathbf{k}) \hat{a}^\dagger(\mathbf{k}) \hat{a}(\mathbf{k}) \hat{a}(\mathbf{k}) \rangle}{\langle \hat{a}^\dagger(\mathbf{k}) \hat{a}(\mathbf{k}) \rangle^2}, \quad (16)$$

and can be calculated using the truncated Wigner method by transforming into symmetric ordering. This correlation function allows us to probe the quantum statistics of each momentum mode – in particular, the occupation statistics in each mode. For coherent, Poissonian statistics  $g^{(2)} = 1$ , and for thermal, Gaussian statistics  $g^{(2)} = 2$ .

We plot  $g^{(2)}(\mathbf{k}, t)$  in Fig. 13 for the state beginning with momentum  $k_L$ . At all times  $g^{(2)}(\pm k_L) \approx 1$ , and the

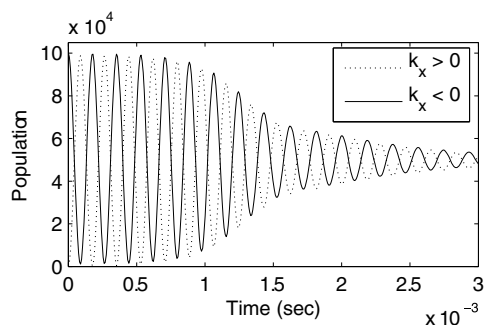


FIG. 14: Time dependence of the total population of all modes with positive or negative momentum in the lattice direction (in the frame of the lattice). These exhibit damped Rabi oscillations in the 2D simulations similar to the 1D results in Fig. 9. Note that onset of damping is more rapid in 2D than 1D, and that revivals are not seen in this case.

condensate modes continue to display coherent statistics. However, we see that the all other populated modes have  $g^{(2)} \approx 2$ . These modes are displaying Gaussian statistics which supports the claim that a thermal cloud is growing around the condensate. Comparing Figs. 12 and 13 we see the modes with phase coherence display second-order coherent statistics and those without phase coherence display thermal statistics. Note again that the noise in Fig. 13 is statistical.

### 4. Rabi oscillations

Finally in Fig. 14 we present results the time dependence of the positive and negative momentum components for the 2D system. These show damped Rabi oscillations with no revivals as observed in in the 1D simulations. There are many more modes in the 2D system, which has two important effects. First, each mode will Rabi oscillate at a different frequency, and so one expects dephasing to wash out the revival. Second, these modes will interact with each other, and the system will approach thermal equilibrium faster. We also see that these the oscillations undergo faster damping compared to the 1D results.

## C. Three Dimensions

### 1. Numerical accuracy

The truncated Wigner method for quantum dynamics is an approximation that is only known to be accurate in certain regimes [55, 58, 59, 60]. It is known to be accurate under the condition that there are many more particles in the simulation than modes. For the experiment we are considering this is difficult to achieve, as in three dimensions the number of modes can easily be greater than one million. Thus, in our calculations we took great care to

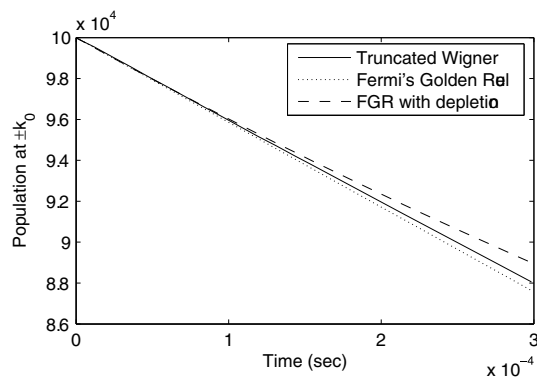


FIG. 15: Condensate occupation of the modes  $\pm\hbar k_L$  versus time for a condensate collision in free space. We compare predictions from truncated Wigner simulations (solid), a straight line fit to the rate given by Fermi's golden rule (dotted), and the solution to the differential equation Eq. (11) that includes condensate depletion (dashed).

use the minimum possible number of modes without misrepresenting the physics. To this end we incorporated a projector to implement a spherical cut-off in momentum space at a radius slightly greater than where the atoms can be expected to be found as estimated from lower-dimensional simulations. A sufficiently large grid was used in real space to eliminate the effects of numerical aliasing [62, 63, 64]. This reduces the number of modes to  $\sim 4 \times 10^5$ , for the simulation of  $10^5$  atoms. The truncated Wigner method will not be accurate for long time scales under these conditions, but we are confident that the dynamics we see in relatively short time scales here is accurate.

We have not implemented the method presented by Polkovnikov [60, 61] to check the validity of our truncated Wigner simulation. Instead, we have tested our accuracy by comparing our simulation of a simple situation with known results. We can compare the spontaneous scattering rates from a simulation with atoms with momentum  $\pm\hbar k_L$  with Fermi's second golden rule, Eq. (11). We have performed this simulation for the same parameters, but without the lattice. The number of atoms remaining in the  $\pm\hbar k_L$  momentum modes is plotted as a function of time in Fig. 15. At small times the results agree well. We can see the effect of Bose-enhancement at later times when Fermi's golden rule underestimates the depletion rate.

## 2. Momentum distribution

In the experiment, time-of-flight expansion was used to image the momentum distributions of the condensates, giving 2D column densities. Fig. 16 shows the results of the three-dimensional calculation where we have summed the populations over the  $z$  momentum component. The ensemble average is for only 32 trajectories due to the

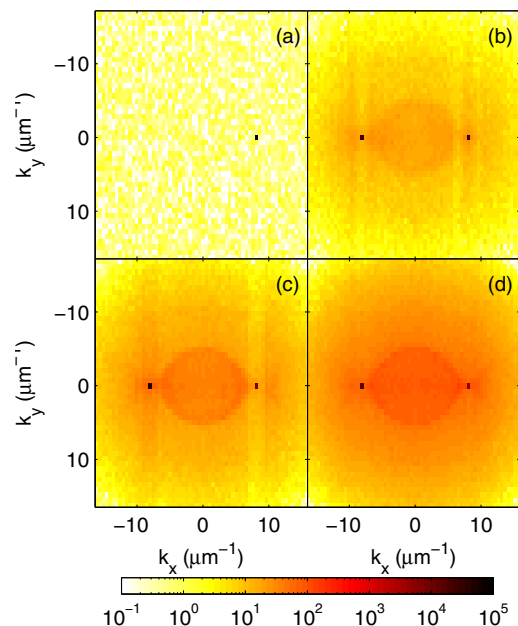


FIG. 16: (Color online) The momentum space column densities for the 3D simulation is shown at times (a) 0 ms, (b) 0.56 ms, (c) 1.1 ms, and (d) 3.0 ms. The scattering halo is clearly visible in (c) and (d).

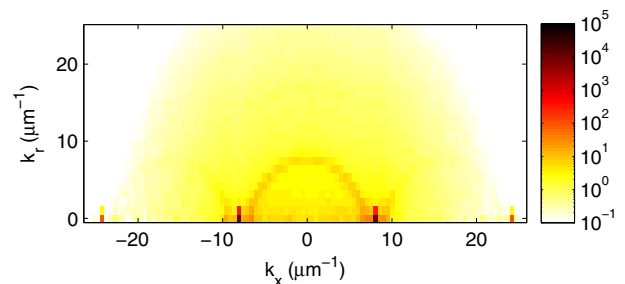


FIG. 17: (Color online) The average population per mode is shown as a function of axial and radial momenta, for a 3D simulation at time 3.0 ms.

computational demands of the simulation. Note that the sharp features seen in the 2D case (Fig. 10) are somewhat washed out, resulting in a distribution more closely resembling two (compact) condensates surrounded by a thermal cloud. However, this is not precisely the case – the population is slightly concentrated in ring-shaped structures in 3D as seen in Fig. 17. These ring-shape structures are similar to those seen in the 2D simulations.

We remind the reader that the simulations performed here are for a homogeneous gas, whereas the condensates in the experiment has a finite momentum width. It seems reasonable to expect that the sharper features would not be as visible in a trapped condensate. In experiments, the expansion is done in finite time which can cause significant broadening of the condensate peaks and other features. Thus, it is reasonable to say there is good qualitative agreement between Fig. 16 and the experimental

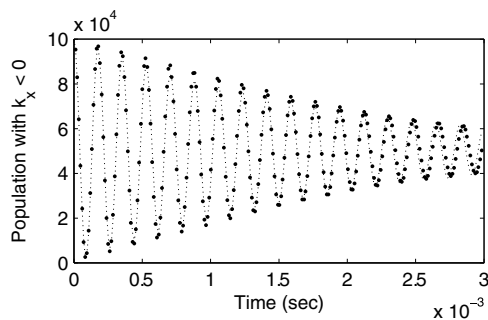


FIG. 18: Population of the momentum modes with  $k_x < 0$  for the 3D simulations. We see damped Rabi oscillations similar to Figs. 9 and 14. A decaying exponential fit (dotted line) has been made with the numerical results (points), with period  $177 \mu\text{s}$  and decay time constant  $2.00 \text{ ms}$ .

images in Fig. 1 when one takes the effects of the trapping potential into account.

### 3. Rabi oscillations

We have plotted the total population with a positive component of momentum in the lattice direction in Fig. 18. An exponentially decaying oscillation of the form

$$P_+ = P_0 \cos(\omega t) e^{-t/\tau} \quad (17)$$

was fitted to the data using a least-squares method. The oscillation period was found to be  $2\pi/\omega = 177 \mu\text{s}$ , as expected for a lattice with  $s = 3.1$ .

The decay constant was found to be  $\tau = 2.00 \text{ ms}$ . This decay is significantly slower than in the experiment, where the decaying fit yields  $\tau = 450 \mu\text{s}$ . There are a number of important experimental considerations that must be accounted for in addition to this result. We shall discuss how to estimate the effects of finite temperature and the momentum spread of the condensate in Sec. VII.

## VII. EXPERIMENTAL CONSIDERATIONS

In this section we consider the effects of the physics that our homogeneous calculations were not able to capture, and estimate their effect on the damping of the Rabi oscillations.

### A. Finite temperature

The simulations we have presented so far have all begun with initial states sampled from the zero temperature Wigner distribution for the condensate. However, if the system is in fact at any non-zero temperature then any surrounding thermal cloud is able to increase the rate of depletion by means of Bose-enhancement of the

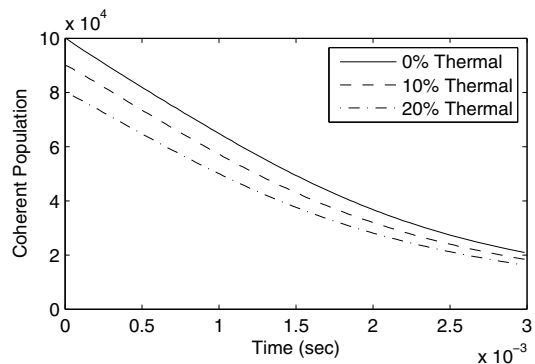


FIG. 19: The total coherent population of the condensate beginning at temperatures corresponding to pure condensate, 90% condensate, and 80% condensate. All simulations contain a total population of  $10^5$  atoms.

resonant collisions. We have performed a 3D simulation with the same parameters as described in Sec. VI C, but with a 10% and 20% thermal fraction surrounding the pure condensate centered with momentum  $+\hbar k_L$ . Note that the experiments began with approximately a 20% thermal fraction.

In Fig. 19 we plot condensate fractions as a function of time. Fermi's golden rule for scattering predicts that the scattering rate is proportional to the square of the number of condensate atoms (*cf.* Eq. (11)). However, such a calculation does not take into account the population of the modes to which atoms are scattered into. A closer look at the results in Fig. 19 indicate that the fractional rate of loss of the coherent component is actually slightly greater in the cases where a thermal cloud is present, after a time of  $200 \mu\text{s}$ . The Bose-enhancement due to the thermal fraction outweighs the reduction in condensate fraction.

The oscillations are also damped more quickly at higher temperatures. An oscillating exponential decay yields damping times of  $\tau \approx 2.00 \text{ ms}$ ,  $1.76 \text{ ms}$ , and  $1.61 \text{ ms}$  for 0%, 10% and 20% thermal fraction respectively. The presence of a thermal fraction can partially account for the faster rates seen in the experiment.

### B. Peak-Density Calculation

Until now our choice of density for the calculations has been the approximate average density of the condensate in the experiment. Here we repeat the simulations using instead the peak density of  $1.7 \times 10^{20} \text{ atoms m}^{-3}$ . We have no *a priori* reason to prefer one over the other. However, as the scattering will occur quickest in the region of highest density, one might expect the dynamics in the peak-density region to dominate.

We performed simulations at zero temperature and with a 20% thermal fraction, finding damping rates of  $1.22 \text{ ms}$  and  $1.00 \text{ ms}$  respectively. These numbers are closer to the experimental results. In the next section we

Description	Density ( $\text{m}^{-3}$ )	Thermal fraction	Damping time
Linear Theory	-	-	954 $\mu\text{s}$
<i>Linear Exp.</i>	-	-	$400 \pm 200 \mu\text{s}$
Truncated Wigner	$1.0 \times 10^{20}$	0%	2.00 ms
Truncated Wigner	$1.0 \times 10^{20}$	10%	1.76 ms
Truncated Wigner	$1.0 \times 10^{20}$	20%	1.61 ms
Truncated Wigner	$1.7 \times 10^{20}$	0%	1.22 ms
Truncated Wigner	$1.7 \times 10^{20}$	20%	1.00 ms
GPE in trap	-	-	1.3 ms
Combined Theory	$1.7 \times 10^{20}$	20%	560 $\mu\text{s}$
<i>Trapped Exp.</i>	-	$\sim 20\%$	$450 \pm 80 \mu\text{s}$

TABLE I: The rates of damping in the simulations and experiments.

combine this with linear dephasing for a full comparison.

### C. Dephasing and Instability

A summary of the results of all our 3D calculations and the experimental results are shown in Table I. We can now combine the results of the linear dephasing and the simulation of the dynamical instability. In the simplest model for decay of the Rabi oscillations, we would simply add the two exponential decay rates by  $\tau^{-1} = \tau_{\text{dephasing}}^{-1} + \tau_{\text{instability}}^{-1}$ . We use the dephasing found in the Gross-Pitaevskii model and instability at the peak density of  $1.7 \times 10^{20} \text{ m}^{-3}$  with a 20% thermal fraction. This results in a decay constant of  $\tau \approx 560 \mu\text{s}$ , which is slightly longer than in the experiment. Given the uncertainties involved in calculating this result we consider that it is in rather good agreement.

## VIII. CONCLUSIONS

In summary, we have described experiments demonstrating the interaction-induced instability of a BEC at

the band-edge of a 1D optical lattice. We have qualitatively studied the effects of dynamical instabilities in one-, two- and three-dimensional systems, demonstrating different regimes of the dynamical instability. We have attempted to quantitatively model the dynamics of this system by using the truncated Wigner method, with good agreement between our experimental and theoretical results.

Our truncated Wigner simulations produced slightly slower scattering and damping of Rabi oscillations than observed in the experiment and showed that the scattering rate is larger for non-zero temperatures. However, in our simulations we have neglected the trapping potential in order find a regime in which the truncated Wigner technique was accurate. We have investigated some of the consequences of the trap using simple linear and mean-field calculations, and found their contribution to damping of Rabi oscillations.

Although the truncated Wigner method has had limitations in the particular experiments presented here, there are many other experiments to which it could be applied. In particular, systems of reduced dimensionality where the condensate is tightly confined in one or two directions (i.e. waveguides) will be well modeled with the truncated Wigner method. This will allow quantitative analysis of non-classical effects in condensates, such as spontaneous scattering, number squeezing effects and entanglement between atoms and with light.

### Acknowledgments

AJF and MJD would like to thank Murray Olsen and Ashton Bradley for useful discussions, and Elena Ostrovskaya for initiating our interest in thermalization in lattices. This work was funded by the Australian Research Council Centre of Excellence for Quantum-Atom Optics and the Marsden Fund of New Zealand.

- 
- [1] M. H. Anderson, J. R. Ensher, M. R. Matthews, C. E. Wieman, and E. A. Cornell, *Science* **269**, 198 (1995).
  - [2] K. B. Davis, M.-O. Mewes, M. R. Andrews, N. J. van Druten, D. S. Durfee, D. M. Kurn, and W. Ketterle, *Phys. Rev. Lett.* **75**, 3969 (1995).
  - [3] C. C. Bradley, C. A. Sackett, J. J. Tollett, and R. G. Hulet, *Phys. Rev. Lett.* **75**, 1687 (1995).
  - [4] Y. B. Ovchinnikov, J. H. Müller, M. R. Doery, E. J. D. Vredenburg, K. Helmerson, S. L. Rolston, and W. D. Phillips, *Phys. Rev. Lett.* **83**, 284 (1999).
  - [5] C. Orzel, A. K. Tuchman, M. L. Fenselau, M. Yasuda, and M. A. Kasevich, *Science* **291**, 2386 (2001).
  - [6] W. K. Hensinger, H. Häffner, A. Browaeys, N. R. Heckenberg, K. Helmerson, C. McKenzie, G. J. Milburn, W. D. Phillips, S. L. Rolston, H. Rubinsztein-Dunlop, et al., *Nature (London)* **412**, 52 (2001).
  - [7] F. S. Cataliotti, S. Burger, C. Fort, P. Maddaloni, F. Minardi, A. Trombettoni, A. Smerzi, and M. Inguscio, *Science* **293**, 841 (2001).
  - [8] M. Greiner, I. Bloch, O. Mandel, T. W. Hänsch, and T. Eslinger, *Appl. Phys. B: Lasers Opt.* **73**, 769 (2001).
  - [9] M. Cristiani, O. Morsch, J. H. Müller, D. Ciampini, and E. Arimondo, *Phys. Rev. A* **65**, 063612 (2002).
  - [10] J. H. Denschlag, J. E. Simsarian, H. Häffner, C. McKen-

- zie, A. Browaeys, D. Cho, K. Helmerson, S. L. Rolston, and W. D. Phillips, *J. Phys. B* **35**, 3095 (2002).
- [11] A. S. Mellish, G. Duffy, C. McKenzie, R. Geursen, and A. C. Wilson, *Phys. Rev. A* **68**, 051601(R) (2003).
- [12] B. Eiermann, T. Anker, M. Albiez, M. Taglieber, P. Treutlein, K.-P. Marzlin, and M. K. Oberthaler, *Phys. Rev. Lett.* **92**, 230401 (2004).
- [13] S. Burger *et al.*, *Phys. Rev. Lett.* **86**, 4447 (2001); B. Wu and Q. Niu, *Phys. Rev. A* **64**, 061603(R) (2001); B. Wu and Q. Niu, *Phys. Rev. Lett.* **89**, 088901 (2002); S. Burger *et al.*, *Phys. Rev. Lett.* **89**, 088902 (2002).
- [14] F. S. Cataliotti, L. Fallani, F. Ferlaino, C. Fort, P. Maddaloni, and M. Inguscio, *New J. Phys.* **4**, 71 (2003).
- [15] M. Cristiani, O. Morsch, N. Malossi, M. Jona-Lasinio, M. Anderlini, E. Courtade, and E. Arimondo, *Opt. Express* **12**, 4 (2004).
- [16] L. Fallani, L. De Sarlo, J. E. Lye, M. Modugno, R. Saers, C. Fort, and M. Inguscio, *Phys. Rev. Lett.* **93**, 140406 (2004).
- [17] L. De Sarlo, L. Fallani, J. E. Lye, M. Modugno, R. Saers, C. Fort, and M. Inguscio, *Phys. Rev. A* **72**, 13603 (2005).
- [18] C. D. Fertig, K. M. O'Hara, J. H. HUCKANS, S. L. Rolston, W. D. Phillips, and J. V. Porto, *Phys. Rev. Lett.* **94**, 120403 (2005).
- [19] N. Katz, R. Ozeri, E. Rowen, E. Gershnel, and N. Davidson, *Phys. Rev. A* **70**, 033615 (2004).
- [20] N. Katz, E. Rowen, R. Ozeri, and N. Davidson, *Phys. Rev. Lett.* **95**, 220403 (2005).
- [21] M. Greiner, O. Mandel, T. Esslinger, T. W. Hänsch, and I. Bloch, *Nature (London)* **415**, 39 (2002).
- [22] F. K. Abdullaev, B. B. Baizakov, S. A. Darmanyan, V. V. Konotop, and M. Salerno, *Phys. Rev. A* **64**, 043606 (2001).
- [23] V. V. Konotop and M. Salerno, *Phys. Rev. A* **65**, 021602(R) (2002).
- [24] B. Wu and Q. Niu, *New J. Phys.* **5**, 104 (2003).
- [25] C. Menotti, A. Smerzi, and A. Trombettoni, *New J. Phys.* **5**, 112 (2003).
- [26] M. Machholm, C. J. Pethick, and H. Smith, *Phys. Rev. A* **67**, 053613 (2003).
- [27] R. G. Scott, A. M. Martin, T. M. Fromhold, S. Bukiewicz, F. W. Sheard, and M. Leadbeater, *Phys. Rev. Lett.* **90**, 110404 (2003).
- [28] M. Machholm, A. Nicolin, C. J. Pethick, and H. Smith, *Phys. Rev. A* **69**, 043604 (2004).
- [29] Y. Zheng, M. Kostrun, and J. Javanainen, *Phys. Rev. Lett.* **93**, 230401 (2004).
- [30] M. Modugno, C. Tozzo, and F. Dalfovo, *Phys. Rev. A* **70**, 043625 (2004).
- [31] F. Nesi and M. Modugno, *J. Phys. B* **37**, S101 (2004).
- [32] M. Modugno, C. Tozzo, and F. Dalfovo, *Phys. Rev. A* **71**, 019904(E) (2005).
- [33] K. Iigaya, S. Konabe, I. Danshita, and T. Nikuni, *Phys. Rev. A* **74**, 053611 (2006).
- [34] A. Polkovnikov, and D.-W. Wang, *Phys. Rev. Lett.* **93**, 070401 (2004).
- [35] L. Isella and J. Ruostekoski, *Phys. Rev. A* **72**, 011601(R) (2005).
- [36] L. Isella and J. Ruostekoski, *Phys. Rev. A* **74**, 063625 (2006).
- [37] J. Ruostekoski, and L. Isella *Phys. Rev. Lett.* **95**, 110403 (2005).
- [38] A. Polkovnikov, E. Altman, E. Demler, B. Halperin, and M. D. Lukin, *Phys. Rev. A* **71**, 063613 (2005).
- [39] J. Gea-Banacloche, A. M. Rey, G. Pupillo, C. J. Williams, and C. W. Clark, *Phys. Rev. A* **73**, 013605 (2006).
- [40] A. M. Rey, G. Pupillo, C. W. Clark, and C. J. Williams, *Phys. Rev. A* **72**, 033616 (2005).
- [41] A. V. Ponomarev and A. R. Kolovsky, *Laser Phys.* **16**, 367-370 (2005).
- [42] E. Altman, A. Polkovnikov, E. Demler, B. I. Halperin, and M. D. Lukin, *Phys. Rev. Lett.* **95**, 020402 (2005).
- [43] N. Gemelke, E. Sarajlic, Y. Bidel, S. Hong, and S. Chu, *Phys. Rev. Lett.* **95**, 170404 (2005).
- [44] K. M. Hilligsøe and K. Mølmer, *Phys. Rev. A* **71**, 041602(R) (2005).
- [45] K. Mølmer, *New. J. Phys.* **8**, 170 (2006).
- [46] G. Campbell, J. Mun, M. Boyd, E. Streed, W. Ketterle, and D. Pritchard, *Phys. Rev. Lett.* **96**, 020406 (2006).
- [47] M. K. Olsen and M. J. Davis, *Phys. Rev. A* **73**, 063618 (2006).
- [48] M. J. Steel, M. K. Olsen, L. I. Plimak, P. D. Drummond, S. M. Tan, M. J. Collett, D. F. Walls, and R. Graham, *Phys. Rev. A* **58**, 4824 (1998).
- [49] C. W. Gardiner and P. Zoller, *Quantum Noise* (Springer, Berlin, 1999), 2nd ed.
- [50] C. W. Gardiner and M. J. Davis, *J. Phys. B* **36**, 4731 (2003).
- [51] B. J. Dąbrowska-Wüster, S. Wüster, A. S. Bradley, M. J. Davis, and E. A. Ostrovskaya, arXiv:cond-mat/0607332 (2006).
- [52] F. Dalfovo, S. Giorgini, L. P. Pitaevskii, and S. Stringari, *Rev. Mod. Phys.* **71**, 463 (1999).
- [53] J. M. Vogels, K. Xu, and W. Ketterle, *Phys. Rev. Lett.* **89**, 020401 (2001).
- [54] A. A. Norrie, R. J. Ballagh, and C. W. Gardiner, *Phys. Rev. Lett.* **94**, 040401 (2005).
- [55] A. A. Norrie, R. J. Ballagh, and C. W. Gardiner, *Phys. Rev. A* **73**, 043617 (2006).
- [56] S. J. Carter, P. D. Drummond, M. D. Reid, and R. M. Shelby, *Phys. Rev. Lett.* **58**, 1841 (1987).
- [57] C. W. Gardiner, *Handbook of Stochastic Methods* (Springer, Berlin, 1985), 2nd ed.
- [58] A. Sinatra, C. Lobo, and Y. Castin, *J. Phys. B* **35**, 3599 (2002).
- [59] P. Deuar and P. D. Drummond, *Phys. Rev. Lett.* **98**, 120402 (2007).
- [60] A. Polkovnikov, *Phys. Rev. A* **68**, 053604 (2003).
- [61] A. Polkovnikov and V. Gritsev, arXiv:0706.0212 (2007).
- [62] M. J. Davis, R. J. Ballagh, and K. Burnett, *J. Phys. B* **34**, 4487 (2001).
- [63] M. J. Davis, S. A. Morgan, and K. Burnett, *Phys. Rev. Lett.* **87**, 160402 (2001).
- [64] M. J. Davis, S. A. Morgan, and K. Burnett, *Phys. Rev. A* **66**, 053618 (2002).
- [65] C. J. Pethick and H. Smith, *Bose-Einstein Condensation in Dilute Gases* (Cambridge University Press, 2001).